Anions of Alkali Halide Salts at Surfaces of Formamide Solutions: Concentration Depth Profiles and Surface Topography

Gunther Andersson,[*1] Harald Morgner,[1] Lukasz Cwiklik,[2] and Pavel Jungwirth[2*]

[1]*Wihelm-Ostwald-Institute for Physical and Theoretical Chemistry Leipzig University, Linnestr.3, 04103 Leipzig, Germany*

[2]*Institute of Organic Chemistry and Biochemistry, Academy of Sciences of the Czech Republic and Center for Biomolecules and Complex Molecular Systems, Flemingovo nám. 2, 16610 Prague 6, Czech Republic*

Keywords: liquid surfaces, topography of surfaces, concentration depth profiles, molecular dynamics simulations, ion scattering spectroscopy

[*] Corresponding Authors: G.Andersson@uni-leipzig.de (G. A.) and Pavel.Jungwirth@uochb.cas.cz (P. J.).

Abstract

Previous computer simulations and surface selective spectroscopic experiments indicated non-monotonic concentration depth profiles for soft inorganic ions (such as iodide) at the air/water interface, while this surface effect was strongly quenched in methanol. Here we investigate by means of neutral impact collision ion scattering spectroscopy and molecular dynamics simulations surface propensity of anions of alkali halide iodide salts in formamide. By combination of experiments and calculations we extract both the ion concentration depth profiles at the interface and the local solvent topography around the ions in or near the top most layer of the liquid. We show that formamide, as a non-aqueous polar solvent containing no hydrophobic groups, exhibits an enhanced surface coverage of soft inorganic ions like iodide and that the ions are located in the outermost layer in valley-like structures. The non-monotonic interfacial concentration profile and surface propensity of iodide in formamide is quantified and compared to that in water.

1. Introduction

The surface structure of solutions containing inorganic salts is a challenging subject in surface science of liquids. The Gibbs equation shows that an increase of the surface tension of a solution with concentration of the solute means that the solute is depleted in the interfacial layer, i.e., the net surface excess of the solute is negative. This is the case for a wide number of solutions of inorganic salts in water.[1] It is, therefore, widely assumed that these solutes are depleted in the outermost layer of aqueous solutions. However, the surface excess is an integral quantity and gives no information about the detailed structure of the surface itself. Thus, by measuring only the surface tension it cannot be determined whether the solute is depleted in the outermost layer or not.[2] Chemical reactions at liquid surfaces or transport over the interface crucially depend on composition of the outermost layer. It is, therefore, important to obtain information about the molecular structure of surfaces of liquid solutions, such as concentration depth profiles and the local surface topography.

For investigation of the molecular structure of liquid surfaces computer simulations must be carried out or experimental methods have to be used that are able to probe the molecular structure directly. Simulations of surfaces of aqueous solutions with inorganic solutes showed that the picture of depletion of inorganic salts in the outermost layer is an oversimplification.[2] Depending on the nature (particularly size and polarizability) of the inorganic ion, depletion or enrichment in the outermost layer was found.[3-5]

Only few experimental techniques are applied to probing directly the molecular structure of liquid surfaces and interfaces. These are neutron reflectivity (NR),[6] X-ray reflectivity (XR),[7,8] nonlinear optical methods (NLO) such as VSFG and SHG,[9,10] several variants of electron spectroscopy (ARXPS[11] and metastable impact electron spectroscopy (MIES)[12]), and ion scattering spectroscopy (i.e., neutral impact collision ion scattering spectroscopy (NICISS)).[13] NR and XR probe the composition of an interface along the z-axis

perpendicular to the surface, while NLO is mainly used to probe the orientation of molecules. In some cases NLO is also used to determine qualitatively the thickness of interfaces, i.e., the thickness of the layer at which the composition and/or orientation differs from that in the bulk.[14] NICISS is used to determine concentration depth profiles of the individual elements at soft matter surfaces[15] and the local topography around elements in a liquid surface.[16]

An interesting question arises whether the surface enhancement observed, e.g. for iodide in water, is present also for non-aqueous inorganic salt solutions. Recently, it has been shown both by MD simulations of the liquid and MIES experiments on the amorphous solid that the ion surface propensity is all but gone in methanol.[17,18] The aim of this paper is to show that at surfaces of solutions with a non-aqueous polar solvent non-monotonic concentration profiles of inorganic salt ions can exist. To this end, we investigate by means of NICISS measurements and computer simulations ion concentration depth profiles and local surface topology for different alkali halides in formamide. We have demonstrated recently that liquid surfaces have interesting inhomogeneous topographies.[16] The local structure can be described as consisting of hills and valleys. We show here that the valley-like structure is found also in present simulations for iodide at the surface of formamide.

2. Methods

Experimental

We have previously investigated surfaces of several pure liquids and surfactant solutions with NICISS.[19-21] This method is used to determine elemental concentration profiles up to a depth of 300 Å with a depth resolution far below 10 Å. The depth resolution of the concentration depth profiles in the outermost layer is given by the accuracy in gauging the zero mark of the depth scale. In deeper layers the blurring of the back scattering angle and the energy straggling limits the resolution.The experimental details are described elsewhere.[20]

The target is bombarded with a pulsed beam of inert gas ions with a kinetic energy of several keV. The energy of the projectiles back scattered from the atoms in the target is determined by their time of flight (TOF) from the target to the detector.

The projectiles lose energy during the back scattering process, which can be described to a good approximation as classical collision between two screened charged hard spheres. The extent of energy transfer depends on the mass of the target atom. Additionally the projectiles loose energy on their trajectory through the bulk with a magnitude proportional to the depth of the target atom due to low angle scattering and electronic excitations (stopping power). The energy loss of the projectiles in the bulk shows a distribution (straggling) since many different processes can lead to the loss of energy. The energy loss in the bulk is calibrated using self assembled monolayers of alkanethiolates on gold and silver single crystals.[15] The depth that can be investigated with this method is limited by the broadening of the beam in the bulk due to low angle scattering. The dose of the He-ions for this investigation was about 10^{10} ions/cm^2. Thus damage of the surface and the influence of the impinging ions on the surface structure can be neglected.

An additional inelastic energy loss occurs during the central scattering event between the projectile and the target atom. This additional energy loss has to be known in order to gauge the zero point of the depth scale.[21] Gas phase NICISS measurements have been performed using diiododemethane to gauge the zero point of the depth scale of iodide and tetrachloromethane to gauge the zero point of the depth scale of chloride.

The liquid surface is generated as a liquid film with a thickness of several tenths of a millimeter on a rotating disk which is partially immersed into a reservoir filled with the investigated liquid. He^+ was used as a projectile. The scattering angle was 168°. The primary energy of the ion beam in our experiments was chosen to be 3.0 keV. The temperature of the solution was set to (278.2 ± 0.2) K.

Surface tensions have been measured with the maximum bobble pressure tensiometer BP2 from Krüss. The solutions have been measured at a temperature of (293.2 ± 0.2) K.

Simulations

The liquid/vapor interface was modeled using molecular dynamics simulations in slab geometry. The unit cell consisted of 500 formamide molecules, to which we added 10 (or 20) sodium cations and 10 (or 20) iodide anions forming a ~0.5 M (or ~1 M) salt solution. In each simulation the system was placed in a 33x33x135 Å rectangular unit cell with periodic boundary conditions in all three directions. This leads to formation of an extended slab with two liquid/vapor interfaces perpendicular to the z-axis. More precisely, the use of 3 D periodic boundary conditions (enabling efficient Ewald summation – *vide infra*) results in a set of identical slabs, which due to the large elongation in the z-direction practically do not interact with each other.[2]

Bonds in formamide molecules were constrained using the SHAKE algorithm.[22] An interaction cut off of 11 Å was employed and the particle mesh Ewald method[23] was used to account for long range electrostatic interactions. Simulations were performed in the canonical constant volume (NVT) ensemble with temperature set to 350 K. The choice of somewhat higher temperature results in a less viscous liquid and, hence, improved sampling of phase space configurations. Equations of motion were integrated with a 2 fs time step. Each system was equilibrated for at least 1 ns (which is sufficient to equilibrate the systems, i.e., the unconstrained degrees of freedom), after which 1 ns production runs followed. All molecular dynamics simulations were performed using the Amber 8 software package.[24]

A polarizable force field was employed in the simulations. Potential parameters for formamide molecules were derived using the Generalized Amber Force Field (GAFF)[25] and the Antechamber program from Amber 8 software package.[26] Additional changes of the

values of partial charges to correct for self-polarization[27] were also taken into account, although they were found to be minor. At the beginning of the parameterization procedure geometry of the formamide molecule was optimized within the density functional theory (DFT) approach employing the B3LYP method with a cc-pVTZ basis set, with the use of the Gaussian03 software package.[28] From this calculation, partial charges were also derived using the electrostatic potential (ESP) method. Next, charges were fitted in Antechamber using the RESP procedure with the self-polarization corrections applied.[27] Standard GAFF values of additional intra- and inter-molecular potential parameters obtained by Antechamber were used. Potential parameters for all atoms and ions are shown in Table 1. The derived potential was tested by comparison to energies from quantum chemical calculations at the B3LYP/aug-cc-pvdz level for formamide-formamide and ion-formamide dimers and by comparing radial distribution functions to those obtained from ab initio molecular dynamics of liquid formamide.

3. Results

Experimental

The surface tension measurements of LiI in formamide show a positive slope of 2.1 ± 0.3 mN m^{-1} kg mol^{-1}. Thus, acording to the Gibbs equation there must be an overall depletion of the solute from the interface of the solutions. This is similar to the situation in aqueous solutions of alkali halide salts [2]. Indeed, the evaluation of the concentration depth profile of iodide yields a negative surface excess (see below).

In Fig. 1 the NICIS spectra of pure formamide, a 0.85 molal solution of LiCl in formamide and a 0.85 molal solution of LiI in formamide are shown. The procedure to determine the spectra of helium back scattered from the different elements is described in detail in Refs. 13 and 20. The measured spectrum of iodide of the 0.85 molal LiI solution

converted to the depth scale is shown in Fig. 2a, while that of chloride of the 0.85 molal LiCl solution is depicted in Fig. 3. The converted spectra are a convolution of the concentration depth profile of the selected element and the energy resolution of the method. The energy resolution is given by the distribution of inelastic energy losses during the back scattering process and the straggling. The distribution of inelastic energy losses during the back scattering process is determined from gas phase spectra.[21] The straggling, which is due to the distribution of inelastic energy losses of the projectile passing through matter, is determined by measuring spectra of aqueous solutions at different vapor pressures.[29] In order to determine the concentration depth profiles of the elements the spectra are deconvoluted with the distribution of inelastic energy losses during the back scattering process and the straggling. The deconvolution is carried out with a program based on a genetic algorithm as described in Ref. 15. The only difference here is that the straggling is also taken into account.

The depth profile of iodide is shown in Fig. 2b and that of chloride in Fig. 3b. The error bars in the deconvoluted profiles are calculated from the statistics of the genetic algorithm, showing thus the spread of the possible different results fitting equally well the measurement. The concentration depth profile of iodide is non-monotonic and shows an enhanced concentration at the surface followed by a minimum below the surface. In Fig. 2c for comparison a fit with a monotonic function is shown. It can be clearly seen that it is not possible to fit the measured spectrum using a monotonic function. This shows that the iodide spectrum can only be fitted with a non-monotonic concentration depth profile. The concentration depth profile of chloride also exhibits slight maximum and a minimum but these are less significant within the error bars than those of the iodide concentration depth profile (Fig. 3b).

The signal due to projectiles back scattered from oxygen and nitrogen can be used to determine concentration depth profiles of the solvent. No changes can be observed in the

concentration depth profile of the solvent upon adding the solute. The change in the concentration depth profile of iodide is up to a factor of 2 as can be seen in Fig 2b and 3b. It can be calculated that in this case the change in the volume fraction of the solvent is less than 3%. Such a small change is hard to observe in the spectra.

The surface excess of the solute can be determined from the concentration depth profiles of the cation. The surface excess of LiI is $(-0.3 \pm 0.2)\ 10^{-10}$ mol/cm^2 and surface excess of LiCl is $(-0.2 \pm 0.2)\ 10^{-10}$ mol/cm^2. Even though the relative error is large a tendency towards a negative surface excess of the solutes can be stated.

Simulations

Force field verification

As a first step, we verified the developed force field. The derived potential parameters were tested in two ways. First, optimized geometries and interaction energies of solvent-solvent and solute-solvent dimer structures were compared with results from DFT calculations. Second, the structural properties (in particular radial distribution functions) of bulk formamide simulated using the present force field were compared to results obtained by ab initio molecular dynamics simulations with interactions described using the BLYP density functional.[30]

The following dimers were considered for testing: i) two formamide molecules (fmm+fmm), ii) a formamide molecule and a sodium cation (fmm+Na^+) , and iii) a formamide molecule and an iodide anion (fmm+I^-). The geometry of each dimer was optimized both with the derived potential parameters and using the B3LYP/aug-cc-pVDZ method. The structures of dimers optimized using the derived potential are presented in Fig. 4 (formamide dimer) and Fig. 5 (formamide-ion dimers). Key interatomic distances are also presented and compared with DFT values. All optimized structures are planar. Most importantly, there is good agreement between the two methods. In Table 2 a comparison of intermolecular interaction

energies of the dimers is presented. Again, the dimer energetic is reproduced well by the empirical potential.

The calculated radial distribution functions of formamide bulk are presented in Fig. 6. The favorable comparison with the distribution functions calculated using ab initio molecular dynamics[30] shows that the derived potential presented here is able to reproduce well the key structural properties of liquid formamide.

Analysis of surface topography

For illustration, Fig. 7 depicts snapshots of surfaces of 0.5 and 1 M NaI in liquid formamide. Qualitatively, we see the presence of iodide at the surface, which increases with concentration but which is smaller than that observed in water previously.[3,31] The snapshots also indicate a certain degree of ion pairing, which is almost absent at these concentrations in water. Increased ion pairing (and decreased salt solubility) is connected with the lower dielectric constant of formamide compared to water.

The solution/vapor interface was further analyzed in terms of density profiles (i.e., distributions of ions across the slab) and the accessible surface area (ASA) of the solute species, i.e., the percentage of the surface covered by the solute.[18,32] Fig. 8a depicts the ion densities of 0.5 M NaI in formamide, from the center of the slab ($z = 0$) across the interface into the gas phase. The same plot for a 1 M solution is shown in Fig. 8b, while Fig. 8c shows results for this system using a non-polarizable force field. In all figures, the solvent (i.e., formamide carbon) density profile is shown as well. The density profiles are normalized such that the integrals of all the curves are the same. We see a pronounced iodide surface peak followed by subsurface depletion and sodium peak in that region. This peak gets smaller with increasing concentration indicating a gradual saturation of adsorption.[33] The ion density profiles are similar to those in water, except that the surface iodide peak is slightly smaller.[31] As in water,[5] the iodide surface effect is strongly diminished by turning to a non-polarizable

potential (Fig. 8c), confirming the key role of polarization interactions for the surface propensity of iodide.

Fig. 9 shows the ASA of iodide in the 0.5 and 1 M formamide solutions. Due to the finite system size the ASA values fluctuate widely during the simulation. Nevertheless, we can estimate that in the former case about 4 % of the surface is covered by iodide while in the later case this number amounts to ~7 %. This value is about half the ASA of iodide in an aqueous solution of a similar concentration[18] indicating less direct surface anionic exposure in formamide. Similarly as in water, the increase of ASA with concentration is slightly sub-linear suggesting again gradual saturation of the surface adsorption sites with increasing number of anions.[33]

Both density profiles and ASA analysis provide a laterally averaged picture of the surface. In order to obtain a more detail information about surface structures around the ions and to assist the interpretation of the experimental data we developed and performed a novel analysis of local surface topography. For each iodide anion in the system a sphere containing neighboring formamide solvent molecules was considered. The radius of the sphere was set equal to that of the first solvation shell (defined as the minimum after the first maximum on the iodide-carbon radial distribution function). Then, the difference $z_{shift} = z_i - z_f$ between the z-coordinate (i.e., the coordinate perpendicular to the surface) z_i of the ion and the mean z-coordinate z_f of the atoms of the formamide molecules in the above defined solvation shell was evaluated. The value of z_{shift} directly characterizes the surface exposure of the ion with respect to the solvent molecules within the first solvation shell, as demonstrated in Fig. 10. This figure depicts several special cases. In the first one, where an ion is in the bulk phase with an intact solvation shell, $z_{shift}=0$ (on average, solvent atoms are placed symmetrically around the ion, therefore, the mean z-coordinate of the solvation shell and that of the ion coincide). Another two characteristic values of z_{shift}, which were also found in the present simulations (see below), are shown in Fig. 10, namely, z_{under} for an ion placed just below the

surface (i.e., touching the surface from the solvent side) and $z_{1/2}$ for a half-exposed ion. Ions can in principle be even more than half-exposed up to the case of an ion just barely touching the surface from outside, as in the most right sketch of Fig. 10. This extreme case has, however, never been observed in the present simulations. The principal advantage of this type of topographic analysis is that it is local and can be, therefore, applied not only to an ideal, flat surface but also to the real, corrugated liquid surface, as schematically shown in Fig. 11. Moreover, results from this analysis can be directly correlated with the present experimental results.

For the present system of sodium iodide in formamide the first solvation shell radius for iodide is 6.2 Å. Then we find z_{under} = 1.1 Å and $z_{1/2}$ = 2.6 Å. Fig. 12 shows as scattered dots the values of z_{shift} as a function of the z-coordinate (depth) for all iodide ions averaged along the MD trajectory for 0.5 M NaI solution in formamide. To guide the eye, we also show the formamide and iodide density profiles, as well as horizontal lines marking the z_{under} and $z_{1/2}$ values. As expected, in the bulk phase the values of z_{shift} are scattered around zero, indicating a complete, symmetric solvation shell around iodide. Moving into the subsurface region there is a markedly reduced density of points, which corresponds to the subsurface depletion of iodide ions. Further toward the surface the number of ions and, therefore, the intensity of the dots increases again with most of the values of z_{shift} being scattered between 0.8 and 2.5 Å. It can be seen that there is a direct correlation between the z-coordinate of an ion and its z_{shift} value. This logically means, that iodide anions closer to the surface tend to be more surface exposed. Moreover, the observed values of z_{shift} of interfacial iodides indicate that the vast majority of the anions in the interface are somewhere between just touching the surface from the solvent side and being half-exposed. In other words, iodide anions tend to sit in valley-like solvent structures at the surface with only a tiny fraction of ions being more than half-exposed. Comparison to analogous results in water (not shown here) indicates that

in formamide anions are less exposed, which is also in accord with the above ASA values for the two solvents.

These observations are further quantified in Fig. 13, where probability distributions of absolute values of z_{shift} are presented. The solid line represents the total distribution, whereas dotted and dashed lines show contributions from layers of solution with a specified depth. The two vertical lines denote the z_{under} and $z_{1/2}$ values. As expected, the deeper layers contribute to lower values of z_{shift}, while the interfacial layers are characterized by larger values of z_{shift}. Note that the total distribution is bimodal, the minimum between the two peaks reflecting again the subsurface depletion of iodide ions.

The depth of the valley like structure in the simulation can be estimated from Fig. 12. The depth is given by the difference of the position on the depth scale of the "center of gravity" of the points marking the z_{shift} of the ions close to the outermost layer ($r > 10.5$ Å) and the position where the density profile of the solution reaches half of the bulk value. The latter represents the average position of the outermost layer with respect to the depth scale. From Fig. 12 we evaluate the position on the depth scale of the above center of z_{shift} as $r = 13.8$ Å with the corresponding mean value of $z_{shift} = 1.6$ Å. The density profile reaches half the bulk value at $r = 15.3$ Å. Thus, the depth of the valley is 1.5 Å (with an estimated error of 0.2 Å).

4. Discussion and Conclusions

We determined concentration depth profiles with ion scattering spectroscopy and by means of computer simulations and found a semiquantitative agreement between the two approaches. It was demonstrated previously that angle resolved ion scattering spectroscopy (ARISS) is able to probe experimentally the topography around ions in the outermost layer of a solution.[16] We have shown that anions are placed in valley-like structures both for salts of cationic surfactants and for inorganic salts. A similar structure of the local topography around

the ions at the surface is found in the results of the computer simulation in the present contribution. The simulations are also capable to analyze the orientation of solute molecules in the interfacial layer. For formamide (unlike, e.g., methanol) the surface orientation is rather weak, with preference of the HCO group to point toward the vapor phase.[34] Similar orientation was also found in experiments by means of MIES [35] and ARISS.[36]

A direct comparison of the ion scattering experiments and the simulation has to take into account the differences in the methods. In the computer simulation the coordinates of the species are given directly while in the case of the experiments they have to be derived from the measurements. As ion scattering spectroscopy shows that the surface of the solution is not flat but exhibits a valley-like structure around the ions, this has to be taken into account in the interpretation of the measured concentration depth profiles. In other words, the ion scattering spectra are determined not only by positions of atoms relative to the surface but also by the local topography of the species at the surface. Thus, the experimental finding of the non-monotonic concentration depth profile of iodide can be caused by two effects. First, there is an increased concentration of iodide in the outermost layer, i.e., the number of iodide molecules in flat layers perpendicular to the z-axis (i.e., parallel with the surface) is enhanced at the outermost one. Second, the maximum and minimum at the depth profile is caused by a local topography effect: an anion at a distance to the averaged outermost layer smaller than a given threshold is not fully covered by solvent molecules, while an ion with a greater distance is fully covered by solvent (Fig. 14). The real situation can also be a combination of both. However, the corrugation of the surface due to the local topography found with ARISS is about 3.3Å and thus much smaller than the maximum and minimum in the concentration depth profile (7±2 Å). Thus we can conclude that the concentration depth profile of iodide is only partially influenced by its local topography at the surface and that the enhanced concentration of iodide in the outermost layer is significant.

The finding of an enhanced iodide concentration in the outermost layer seems to be in odds with the thermodynamic result that there is an overall depletion of the solute at the surface. Reconcilliation lies in the fact that the negative surface excess as an integral quantity can results from a non-monotoneous concentration depth profile [2]. Indeed, the surface excess determined form the concentration depth profiles is negative both for LiI and LiCl, since the maximum in the outermost layer is more than compensated by the minimum in the solute concentration in the subsurface region (in the simulations, due to finite system size, this compensation is not fully quantitative).

The depth of the valley like structure in which the iodide is located in the outermost layer is smaller in the simulation (1.5 Å) than in the experiment (3.3 Å). It should be noted that in the simulation the local structure is taken into account only up to the first solvation shell of the iodide. Thus, this quantitative discrepancy may be largely due to slightly different definitions of the depth of the valley like structure in the experiment and simulation.

In the simulations a somewhat higher temperature was used in order to enhance statistical sampling in a relatively viscous liquid such as formamide. We expect that the influence of the temperature is of minor importance but this shall be subject of future investigations. It can be expected, that the direct accessibility of iodide to the gas phase is more pronounced for higher temperatures, since the hydration number of halide ions decreases slightly with increasing temperature in aqueous solutions.[37] Also, we used sodium instead of lithium iodide in the simulations knowing that the effect of different alkali counter cations on the studied properties is very small.[2] In addition, performed preliminary calculations on sodium chloride in formamide which showed a significantly reduced anionic surface peak compared to iodide, in agreement with experiment. However, due to low solubility of NaCl in formamide and inaccuracies in the force field the simulations suffered from extensive ion pairing and clustering. This resulted in poor statistical sampling, therefore, we do not report these results here in detail.

Finally, it is illuminating to compare the present results to simulations of alkali iodide salts in methanol[17,18] and water.[18,31] In methanol, on one hand, the iodide surface propensity is all but gone due to the fact that the top most layer of the solution is plagued with hydrophobic methyl groups.[18] On the other hand, the iodide density profiles in the two solvents not containing any hydrophobic groups (i.e., formamide and water) exhibit a strongly non-monotonic behavior and are very similar to each other with the surface peak of I^- being only slightly less pronounced in formamide than in water. However, there is a significant difference in surface exposure with the accessible surface area of iodide being roughly twice as large in water than in formamide at comparable concentrations.[18] This is due to the fact that the valley-like solvent structures around iodide are less deep in water than in formamide.

Acknowledgment

We want to thank Mrs. A. Förster for measuring the surface tension. Support from the Czech Ministry of Education (Grants LC512 and ME644) is gratefully acknowledged. Part of the work in Prague was completed within the framework of the Research Project Z40550506. We acknowledge also the support of the German Science Foundation (DFG Mo 288/25).

References

[1] Matubayasi, N.; Tsunetomo, K.; Sato, I.; Akizuki, R.; Morishita, T.; Matuzawa, A.; Natsukari, Y. *J. Col. Int. Sci.*, **2001**, *243*, 444.

[2] Jungwirth, P.; Tobias, D. J. *Chem. Rev.*, **2006**, *106*, 1259.

[3] Jungwirth, P.; Tobias, D. J. *J. Phys. Chem.* B **2002**, *106*, 6361.

[4] Dang, L. X. *J. Phys. Chem.* B **2002**, *106*, 10388.

[5] Vrbka, L.; Mucha, M.; Minofar, B.; Jungwirth, P.; Brown, E. C.; Tobias, D. J. *Curr. Opin. Colloid Interface Sci.* **2004**, *9*, 67.

[6] Lu, J. R.; Thomas, R. K.; Penfold, J. *Adv. Col. Int. Sci.*, **2000** , *84*, 143.

[7] Zhang, Z.; Mitrinovic, D.; Williams, S. M.; Huang, Z.; Schlossman, M. L. *J. Chem Phys.* **1999**, *110*, 7421.

[8] Penfold, J. *Rep. Prog. Phys.* **2001**, *64*, 777.

[9] Richmond, G. L. *Chem Rev.* **2000**, *102*, 2693.

[10] Wei, X.; Shen, Y. R. *Phys. Rev. Lett.* **2001**, *86*, 4799.

[11] Eschen, F.; Heyerhoff, M.; Morgner, H.; Vogt, J. *J. Phys. Cond. Mat.* **1995**, *7*, 1961.

[12] Morgner, H. *Adv. Atom. Mol. Opt. Phys.* **2000**, *42,* 387.

[13] Andersson, G.; Krebs, T.; Morgner, H. *Phys. Chem. Chem. Phys*., **2005**, *7*, 136.

[14] Gopalakrishnan, S.; Jungwirth, P.; Tobias, D. J.; Allen, H. C. *J. Phys. Chem. B*, **2005**, *109*, 8861.

[15] Andersson, G.; Morgner, H. *Nucl. Instrum. Methods Phys. Res., Sect. B*, **1999**, *4*, 357.

[16] Andersson, G.; Krebs, T.; Morgner, H. *Phys. Chem. Chem. Phys.* **2005**, *7*, 2948.

[17] Dang, L. X. *J. Phys. Chem. A*, **2004**, *108*, 9014.

[18] Hoefft, O.; Borodin, A.; Kahnert, U.; Kempter, V.; Dang, L. X.; Jungwirth, P. *J. Phys. Chem. B*, **2006**, *110*, 11971.

[19] Andersson, G.; Morgner, H. *Surf. Sci.* **1998**, *405*, 138.

[20] Andersson, G.; Morgner, H. *Surf. Sci.* **2000**, *445*, 89.

[21] Andersson, G.; Morgner, H.; Schulze, K. D. *Nucl. Instrum. Methods Phys. Res., Sect. B*, **2002**, *190*, 222.

[22] Ryckaert, J.-P.; Ciccotti, G.; Berendsen, H. J. C J. Comp. Phys. **1977**, *23*, 327.

[23] Essmann, U.; Perera, L.; Berkowitz, M. L.; Darden, T.; Pedersen, L. G. J. Chem. Phys. **1995**, *103*, 8577.

[24] Case, D. A.; Darden, T. A.; Cheatham, III, T. E.; Simmerling, C. L.; Wang, J.; Duke, R. E.; Luo, R.; Merz, K. M.; Wang, B.; Pearlman, D. A.; Crowley, M.; Brozell, S.; Tsui, V.; Gohlke, H.; Mongan, J.; Hornak, V.; Cui, G.; Beroza, P.; Schafmeister, C.; Caldwell, J. W.; Ross, W. S.; Kollman P. A. *Amber 8*, University of California, San Francisco, 2004.

[25] Wang, J., Wolf, R. M.; Caldwell, J. W.;Kollman, P. A.; Case, D. A. *J. Comput. Chem.* **2004**, *25*, 1157.

[26] Wang, J., Wang, W., Kollman P. A.; Case, D. A. *J. Mol. Graphics Modelling* **2006**, *25*, 247260.

[27] Cieplak, P.; Caldwell, J.; Kollman, P. A. *J. Comput. Chem.* **2001**, *22*, 1048.

[28] Frisch, M. J.; Trucks, G. W.; Schlegel, H. B.; Scuseria, G. E.; Robb, M. A.; Cheeseman, J. R.; Montgomery, Jr., J. A.; Vreven, T.; Kudin, K. N.; Burant, J. C.; Millam, J. M.; Iyengar, S. S.; Tomasi, J.; Barone, V.; Mennucci, B.; Cossi, M.; Scalmani, G.; Rega, N.; Petersson, G. A.; Nakatsuji, H.; Hada, M.; Ehara, M.; Toyota, K.; Fukuda, R.; Hasegawa, J.; Ishida, M.; Nakajima, T.; Honda, Y.; Kitao, O.; Nakai, H.; Klene, M.; Li, X.; Knox, J. E.; Hratchian, H. P.; Cross, J. B.; Bakken, V.; Adamo, C.; Jaramillo, J.; Gomperts, R.; Stratmann, R. E.; Yazyev, O.; Austin, A. J.; Cammi, R.; Pomelli, C.; Ochterski, J. W.; Ayala, P. Y.; Morokuma, K.; Voth, G. A.; Salvador, P.; Dannenberg, J. J.; Zakrzewski, V. G.; Dapprich, S.; Daniels, A. D.; Strain, M. C.; Farkas, O.; Malick, D. K.; Rabuck, A. D.; Raghavachari, K.; Foresman, J. B.; Ortiz, J. V.; Cui, Q.; Baboul, A. G.; Clifford, S.; Cioslowski, J.; Stefanov, B. B.; Liu, G.; Liashenko, A.; Piskorz, P.; Komaromi, I.; Martin, R. L.; Fox, D. J.; Keith, T.; Al-Laham, M.

A.; Peng, C. Y.; Nanayakkara, A.; Challacombe, M.; Gill, P. M. W.; Johnson, B.; Chen, W.; Wong, M. W.; Gonzalez, C.; and Pople, J. A. *Gaussian 03*, Gaussian, Inc., Wallingford CT, 2004.

[29] Andersson, G. *submitted.*

[30] Tsuchida, E. *J. Chem. Phys.* **2004**, *121*, 4740.

[31] Jungwirth, P.; Tobias, D. J. *J. Phys. Chem.* B **2001**, *105*, 10468.

[32] Lee, B.; Richards, P. M. *J. Mol. Biol.* **1971**, *55*, 379.

[33] Petersen, P. B.; Mucha,M.; Jungwirth, P.; Saykally, R. J., *J. Phys. Chem. B*, **2005**, *109*, 10915.

[34] Oberbrodhage, J.; Morgner, H.; Tapia, O.; Siegbahn, H. O. C., *Int. J. Quantum Chem.*, **1997**, *63*, 1123.

[35] W. Keller, H. Morgner and W.A. Müller, *Mol. Phys.*, **1986**, *57*, 623.

[36] G. Andersson, *Phys. Chem. Chem. Phys.*, **2005**, *7*, 2942.

[37] Zavitsas, A. A., *J. Phys. Chem. B*, **2001**, *105*, 7805.

Tables:

Table 1. Force field parameters of atoms and ions used in the present work. Hydrogen atoms in formamide molecule were labeled in the following way: H_F – hydrogen in the CHO group, H_C – hydrogen in the NH_2 group in the *cis* position with respect to oxygen atom, H_T – hydrogen in the NH_2 group in the *trans* position with respect to oxygen atom.

atom/ ion	GAFF atom type	charge [e]	polarizability [Å ^{3}]	vdW radius [Å]	vdW well depth [kcal/mol]
O	o	-0.548	0.434	1.661	0.210
C	c	0.613	0.616	1.908	0.860
H_F (-CHO)	h5	-0.016	0.135	1.359	0.015
N	n	-0.834	0.530	1.824	0.170
H_C (cis O)	hn	0.411	0.161	0.600	0.016
H_T (trans O)	hn	0.374	0.161	0.600	0.016
Na+	-	1.000	0.240	1.319	0.130
I-	-	-1.000	6.900	2.890	0.100

Table 2: Interaction energies of the formamide-formamide, formamide-sodium, and formamide-iodide dimmers obtain from the present empirical force field, compared to DFT/B3LYP values.

Dimmer	GAFF energy [kcal/mol]	DFT energy [kcal/mol]
fmm+fmm	-13.2	-14.3
fmm+Na^+	-35.7	-29.7
fmm+I^-	-15.8	-13.8

Figure captions:

Fig. 1: TOF-spectra from pure formamide (a), a 0.85 molal solution of LiCl in formamide (b) and a 0.85 molal solution of LiI in formamide.

Fig. 2: (a) Concentration depth profile of iodide as directly converted from the TOF scale to the depth scale and (b) deconvolution of the concentration depth profile. In (b) we show also the measured and the fitted curves. The latter is a back convolution of the deconvoluted curve, which fits well the measurement. For comparison, in (c) a fit with a monotonic function is shown. It can be clearly seen that it is not possible to fit the measured spectrum using a monotonic concentration depth profile.

Fig. 3: : (a) Concentration depth profile of chloride as directly converted from the TOF scale to the depth scale and (b) deconvolution of the concentration depth profile. In (b) we show also the measured and the fitted curves. The latter is a back convolution of the deconvoluted curve, which fits well the measurement.

Fig. 4: Geometry of formamide dimer optimized using the derived force field (distances given in Angstroms). Interatomic distances from B3LYP/aug-cc-pvdz optimization are presented in parenthesis.

Fig. 5: Geometries of dimers of formamide with (A) iodide anion and (B) sodium cation optimized with the derived force field (distances given in Angstroms). Interatomic distances from B3LYP/aug-cc-pvdz optimizations are presented in parenthesis.

Fig. 6: Radial distribution functions for all atomic pairs in liquid formamide simulated using the derived force field. The notation of the hydrogen atoms is the same as in Table 1.

Fig. 7: Representative snapshots from molecular dynamics simulations of the surfaces of a) 0.5 M and b) 1 M solution of NaI in formamide. Color coding: iodide – pink, sodium – green, oxygen – red, nitrogen – blue, carbon – cyan, and hydrogen – white.

Fig. 8: Density profiles, i.e., distributions of sodium and iodide ions, as well as carbon atoms of formamide, from the center of the slab across the solution/vapor interface into the gas

phase. Results for a) 0.5 M solution, b) 1 M solution, and c) 1 M solution with a non-polarizable force field.

Fig. 9: Accessible surface area, i.e., percentage of the surface covered by iodide anions during the MD simulation. a) 0.5 M and b) 1 M NaI solution in formamide.

Fig. 10: A schematic picture showing the ion (brown) with the first solvation shell (green) at different distances from the surface of a liquid (blue). The corresponding values of z_{shift} are also indicated.

Fig. 11: A sketch of different positions of the ion (brown) and its first solvations shell (green) with respect to a corrugated liquid surface (blue).

Fig. 12: Values of z_{shift} shown as scattered dots as function of the z-coordinate (depth) for all iodide ions averaged along the MD trajectory for the 0.5 M NaI solution in formamide. Water and iodide density profiles, as well as horizontal lines marking the z_{under} and $z_{1/2}$ values of z_{shift} are also shown.

Fig. 13: Probability distributions of absolute values of z_{shift} for iodide. The thick solid line is the total distribution and the thick dashed line is the integral thereof. Thin dotted and dashed lines depict contributions from layers of solution with a specified depth. The two vertical lines denote the z_{under} and $z_{1/2}$ values of z_{shift}. Results correspond to the 0.5 M NaI solution in formamide.

Fig. 14: Illustration of the two different ion topographies for possible explanations of the experimentally measured concentration depth profile: (a) an anion located relative to the outermost layer (average outermost layer) at a distance less than the threshold d_{min} is solvated only partially, i.e. not covered by solvent molecules in the direction towards the gas phase. (b) An anion located relative to the outermost layer (average outermost layer) at a distance greater than the threshold d_{min} is solvated fully.

Figures:

Fig. 1

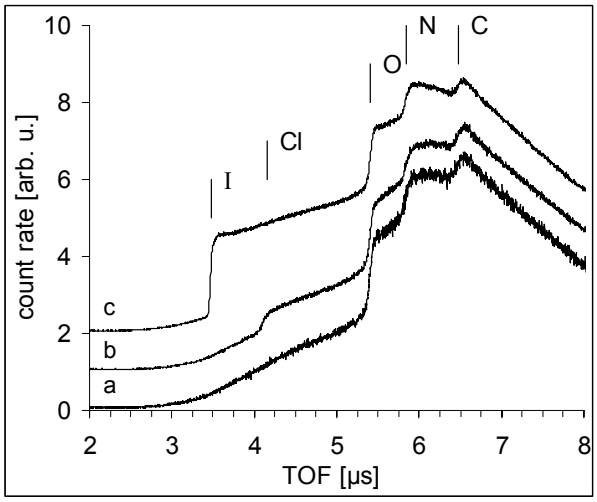

Fig. 2a

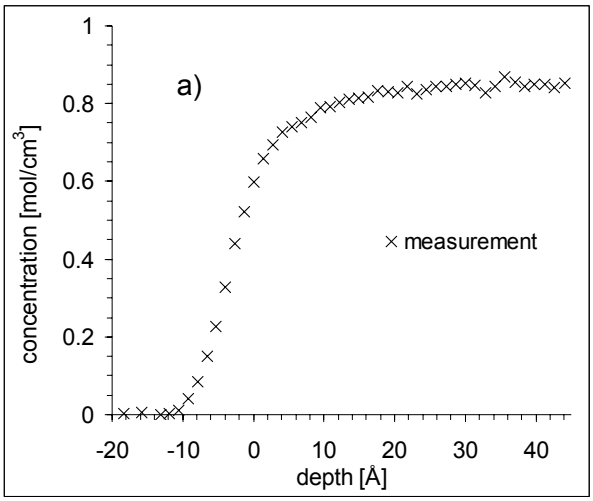
a)
concentration [mol/cm3]
depth [Å]
measurement
1
0.8
0.6
0.4
0.2
0
-20
-10
0
10
20
30
40

Fig. 2b

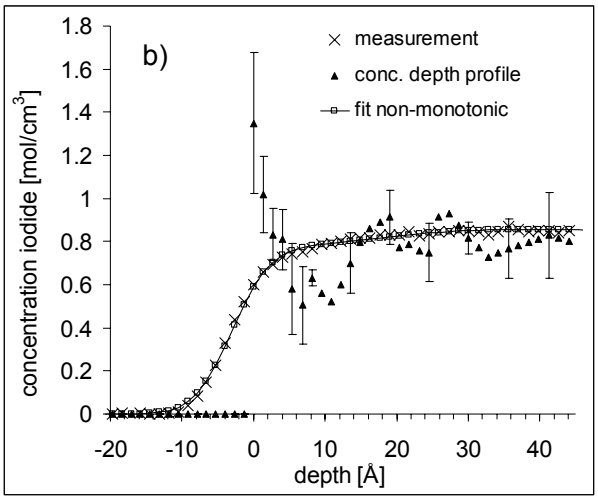
b)
measurement
conc. depth profile
fit non-monotonic
concentration iodide [mol/cm3]
depth [Å]
1.8
1.6
1.4
1.2
1
0.8
0.6
0.4
0.2
0
-20
-10
0
10
20
30
40

Fig. 2c

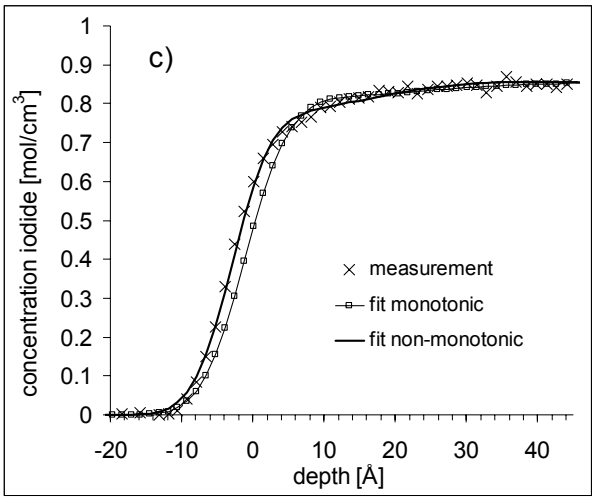
c)
concentration iodide [mol/cm3]
depth [Å]
measurement
fit monotonic
fit non-monotonic
1
0.9
0.8
0.7
0.6
0.5
0.4
0.3
0.2
0.1
0
-20
-10
0
10
20
30
40

Fig. 3a

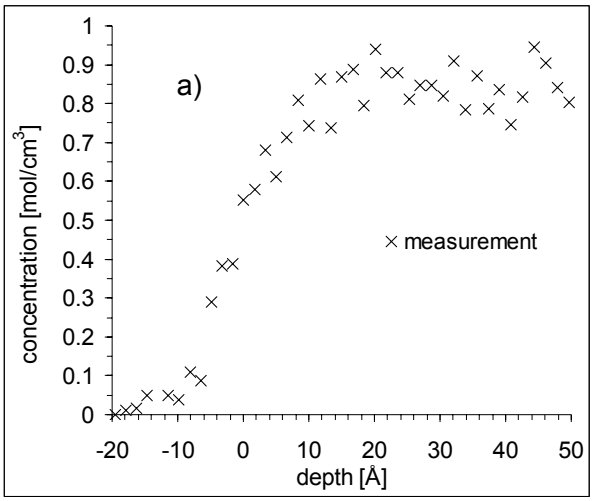
a)
concentration [mol/cm3]
depth [Å]
measurement
1
0.9
0.8
0.7
0.6
0.5
0.4
0.3
0.2
0.1
0
-20
-10
0
10
20
30
40
50

Fig. 3b

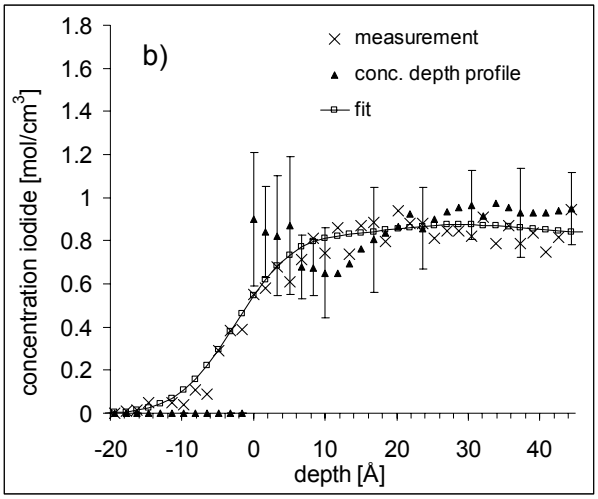
b)
measurement
conc. depth profile
fit
concentration iodide [mol/cm3]
depth [Å]
1.8
1.6
1.4
1.2
1
0.8
0.6
0.4
0.2
0
-20
-10
0
10
20
30
40

Fig. 4

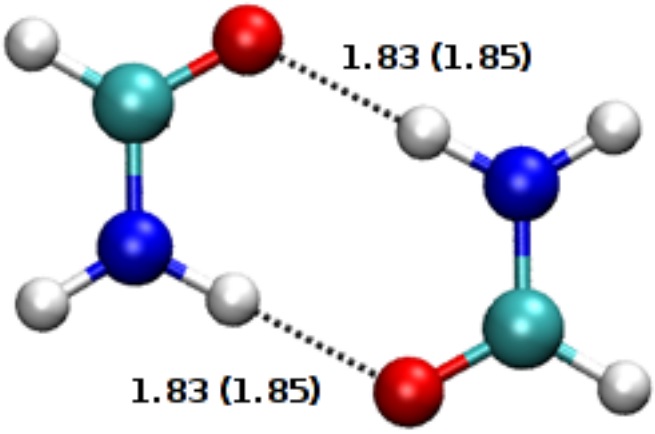

Fig. 5

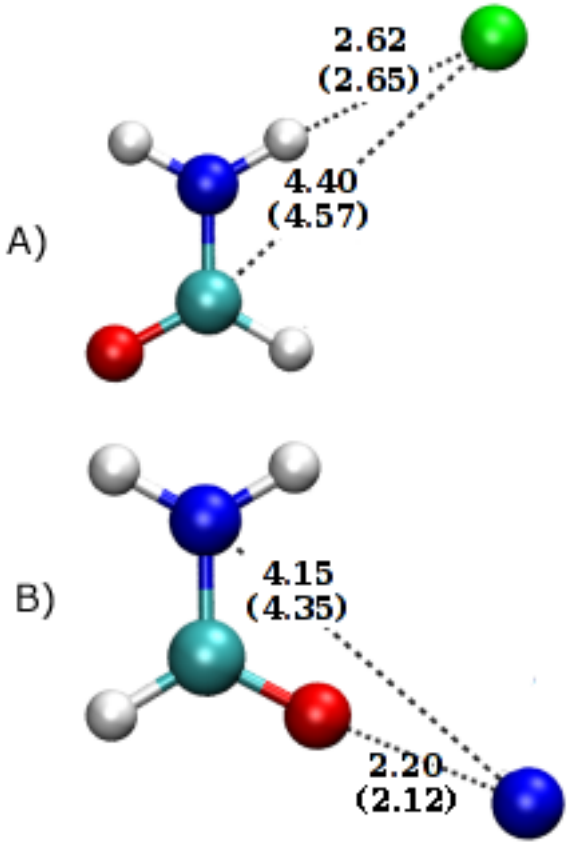

Fig. 6

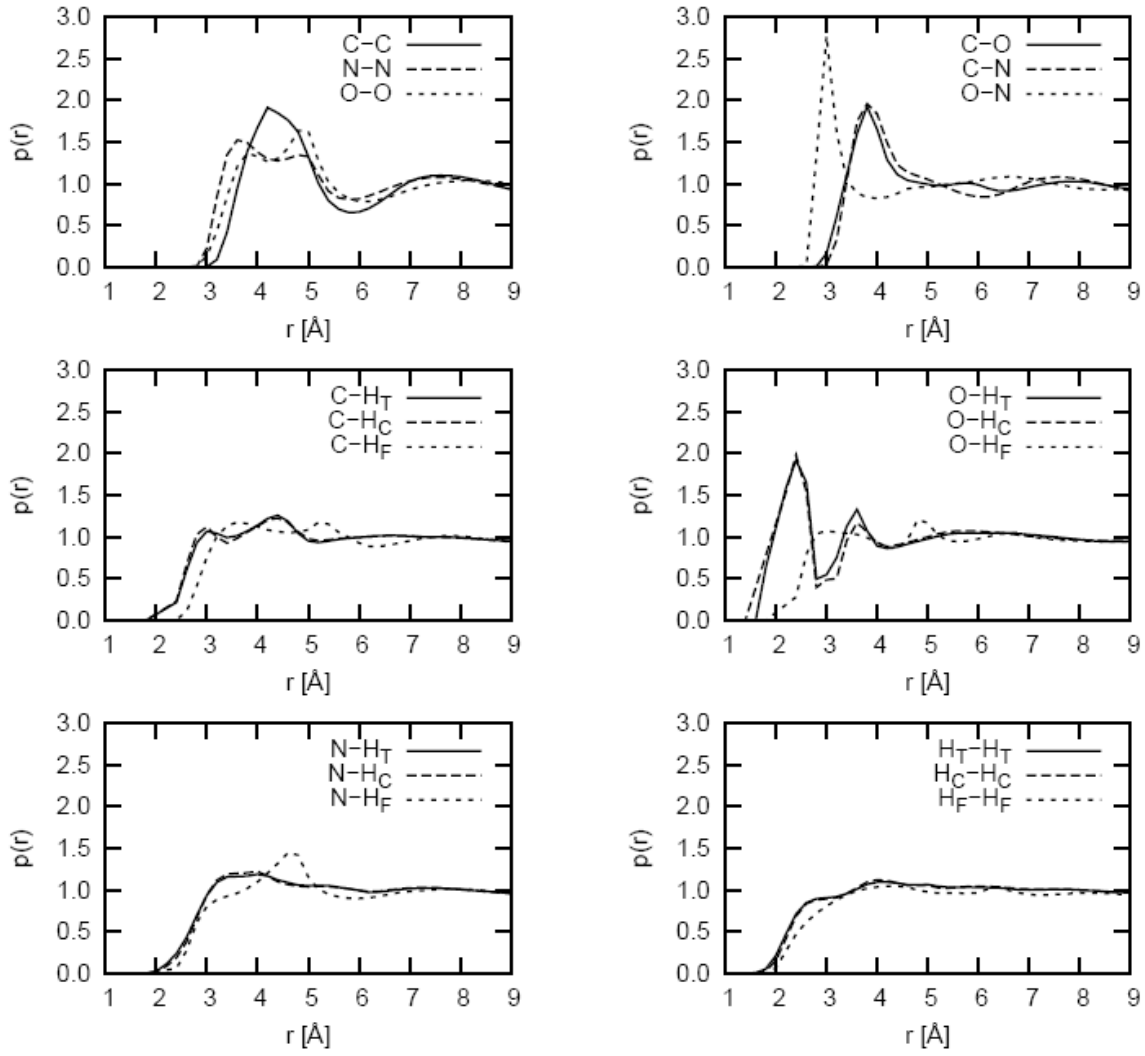
C–C
N–N
O–O
C–O
C–N
O–N
C–H$_T$
C–H$_C$
C–H$_F$
O–H$_T$
O–H$_C$
O–H$_F$
N–H$_T$
N–H$_C$
N–H$_F$
H$_T$–H$_T$
H$_C$–H$_C$
H$_F$–H$_F$
p(r)
r [Å]

Fig. 7a

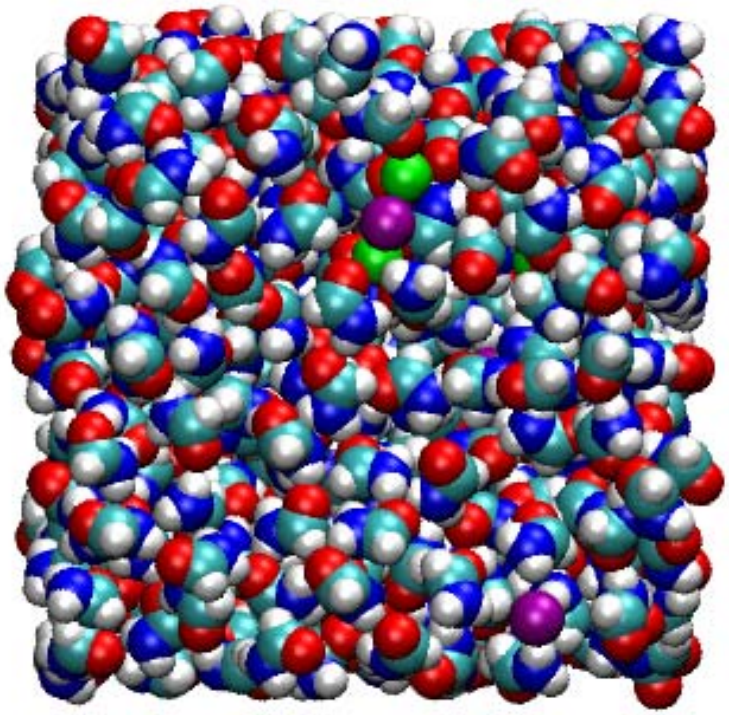

Fig. 7b

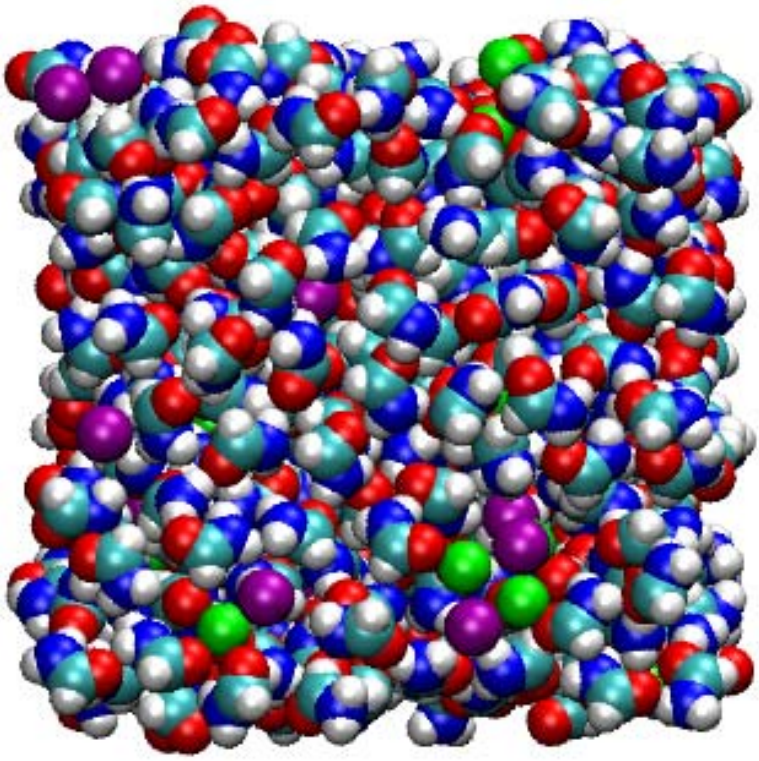

Fig. 8a

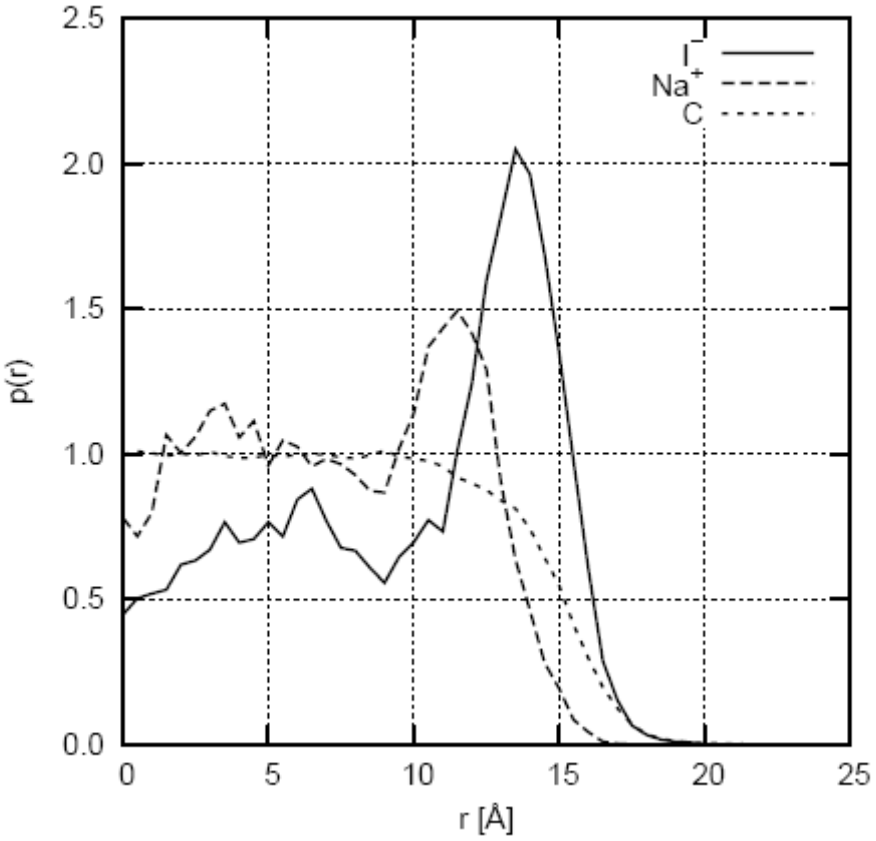

Fig. 8b

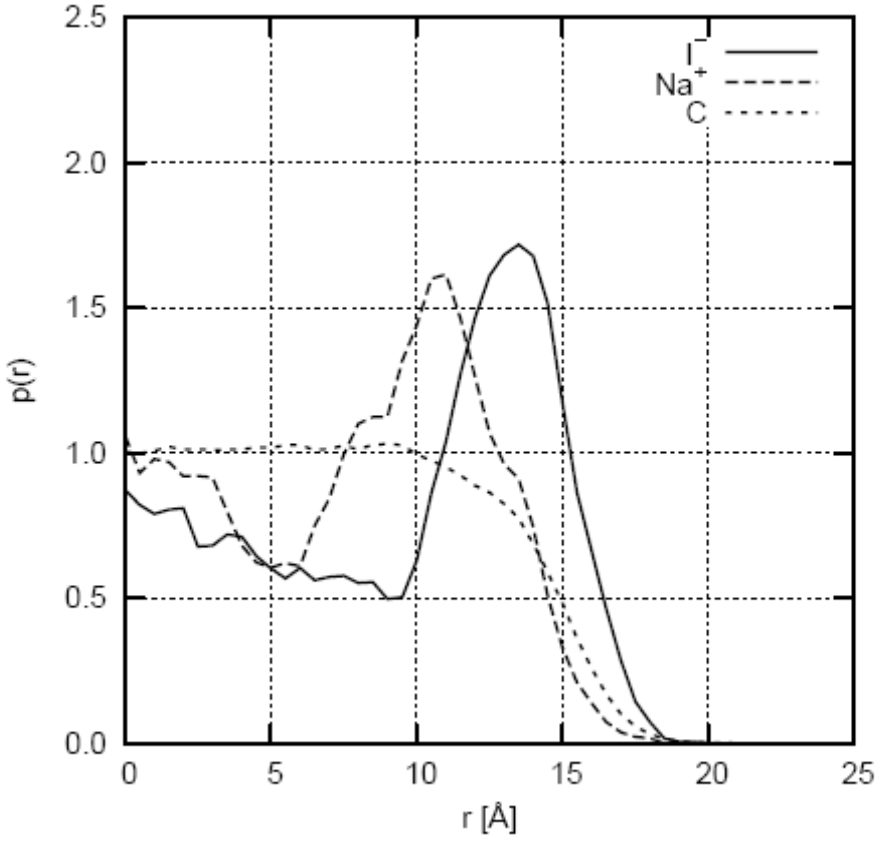

Fig. 8c

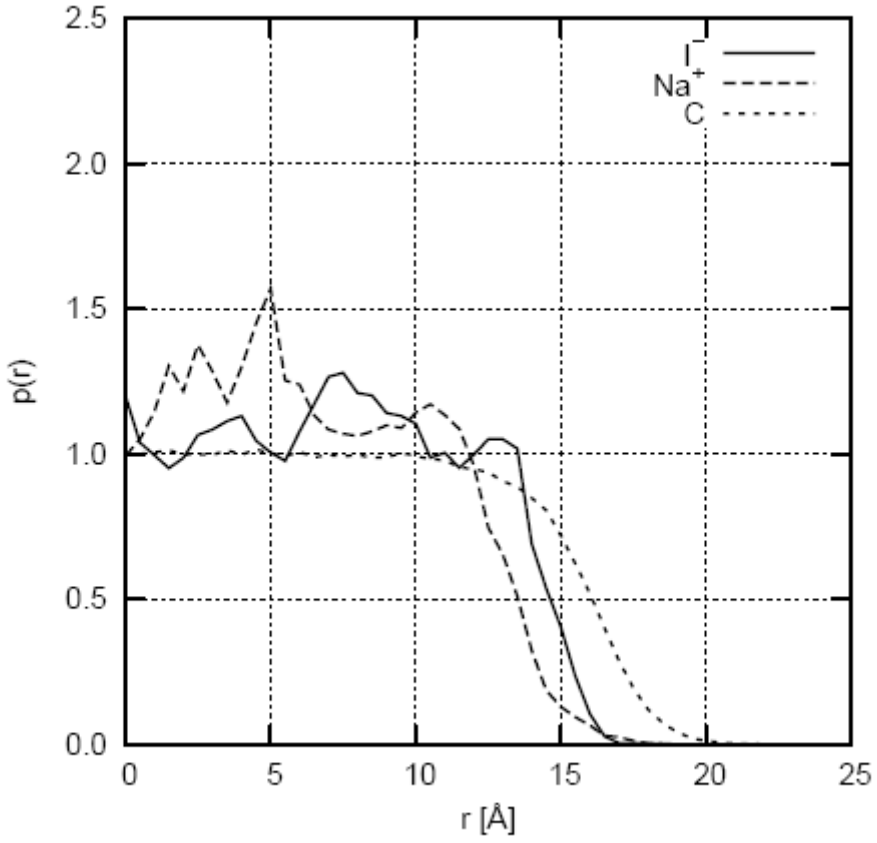

Fig. 9a

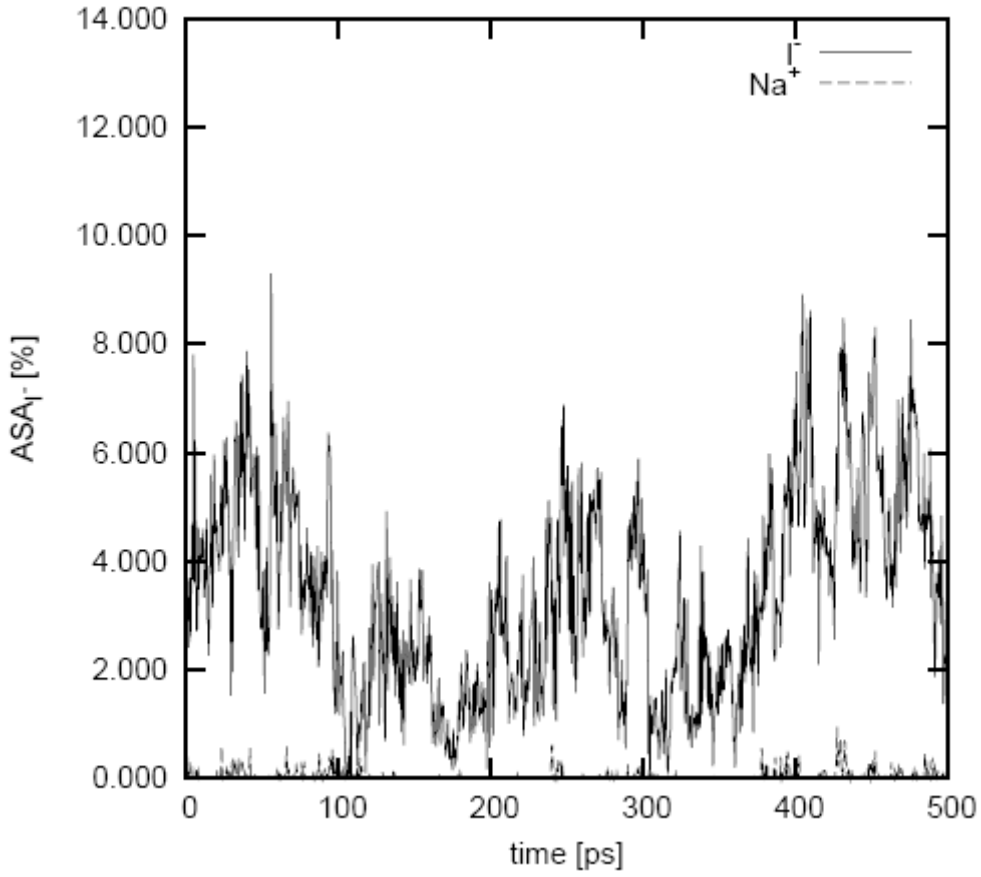
14.000
12.000
10.000
8.000
6.000
4.000
2.000
0.000
ASA$_{I^-}$ [%]
0
100
200
300
400
500
time [ps]
I$^-$
Na$^+$

Fig. 9b

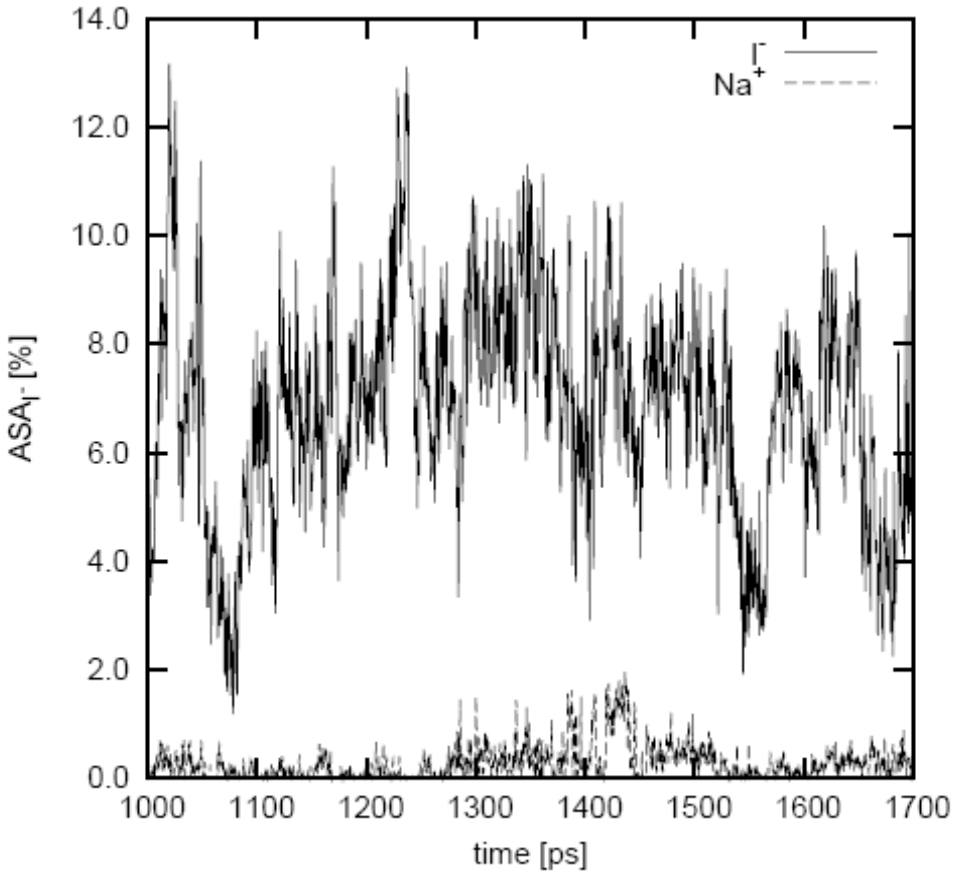
14.0
12.0
10.0
8.0
6.0
4.0
2.0
0.0
1000
1100
1200
1300
1400
1500
1600
1700
time [ps]
ASA$_{I^-}$ [%]
I$^-$
Na$^+$

Fig. 10

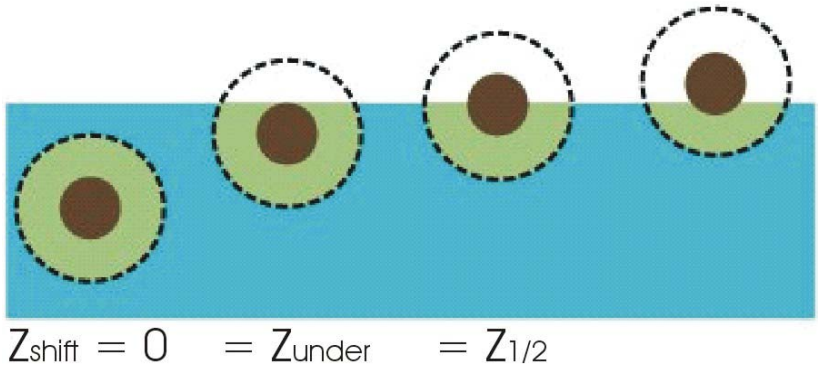

Fig. 11

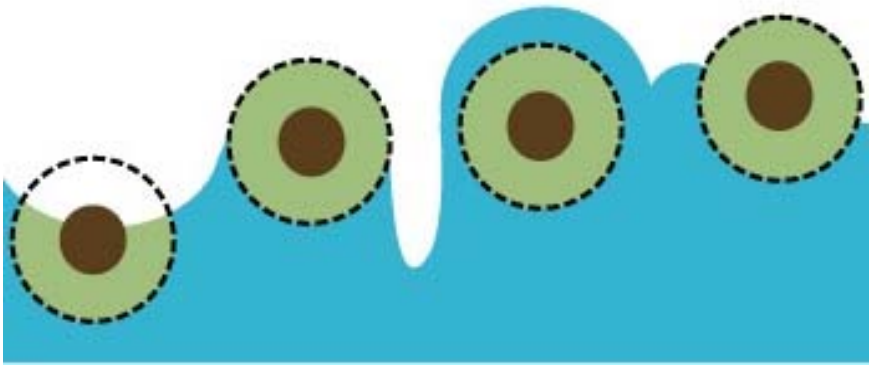

Fig. 12

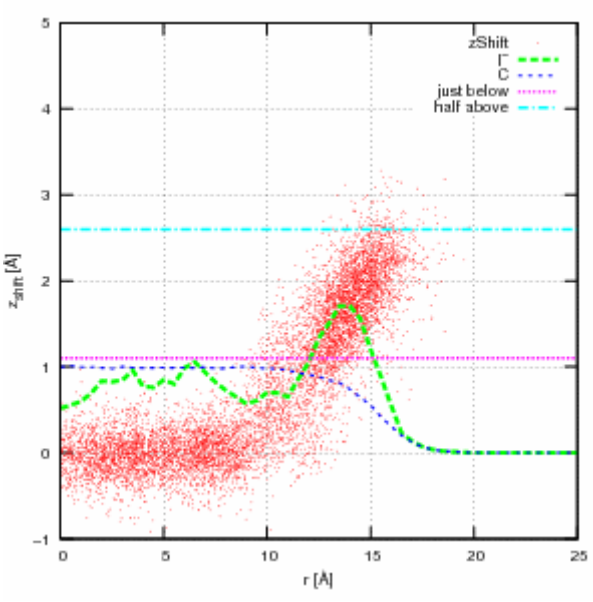
zShift
Γ
C
just below
half above
z_shift [Å]
r [Å]
5
4
3
2
1
0
−1
0
5
10
15
20
25

Fig. 13

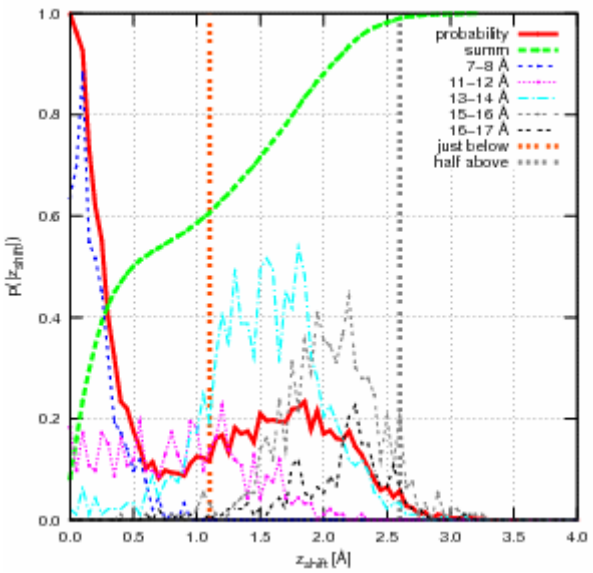
probability
summ
7–8 Å
11–12 Å
13–14 Å
15–16 Å
16–17 Å
just below
half above
1.0
0.8
0.6
0.4
0.2
0.0
0.0
0.5
1.0
1.5
2.0
2.5
3.0
3.5
4.0
P(|z_shift|)
z_shift [Å]

Fig. 14a

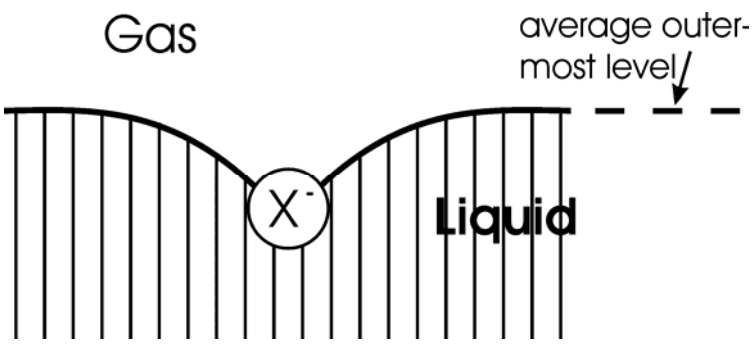

Fig. 14b